SUPPLEMENTARY INFORMATION

Table S1: Summary of purification yields of WT and mutant BECN2 CCDs.

BECN2 CCD	Yield (mg per liter cells)
Wild type	0.9
E173L	0.8
N187L	3.8
A190L+Y215L	2.9
A197L+E208L	4.7
H211L	1.8
Q222L	0.6
R243L	0.6

Table S2: CD Analysis of Secondary Structure Content of the 98-Residue WT and Mutant BECN2 CCDs.

BECN2 CCD	Helix (residues)	Strand (residues)	Turn + Coil (residues)
Wild type	71 ± 4	0 ± 0	28 ± 4
E173L	77 ± 5	0 ± 0	21 ± 4
N187L	85 ± 10	-1 ± 1	13 ± 10
A190L+Y215	78 ± 3	-1 ± 1	20 ± 3
A197L+E208L	83 ± 4	-1 ± 1	16 ± 6
H211L	81 ± 6	-1 ± 1	17 ± 6
Q222L	72 ± 1	0 ± 0	26 ± 1
R243L	78 ± 2	0 ± 0	21 ± 2

The number of residues reported are averages of estimates from SELCON3[1] and K2D3[2].

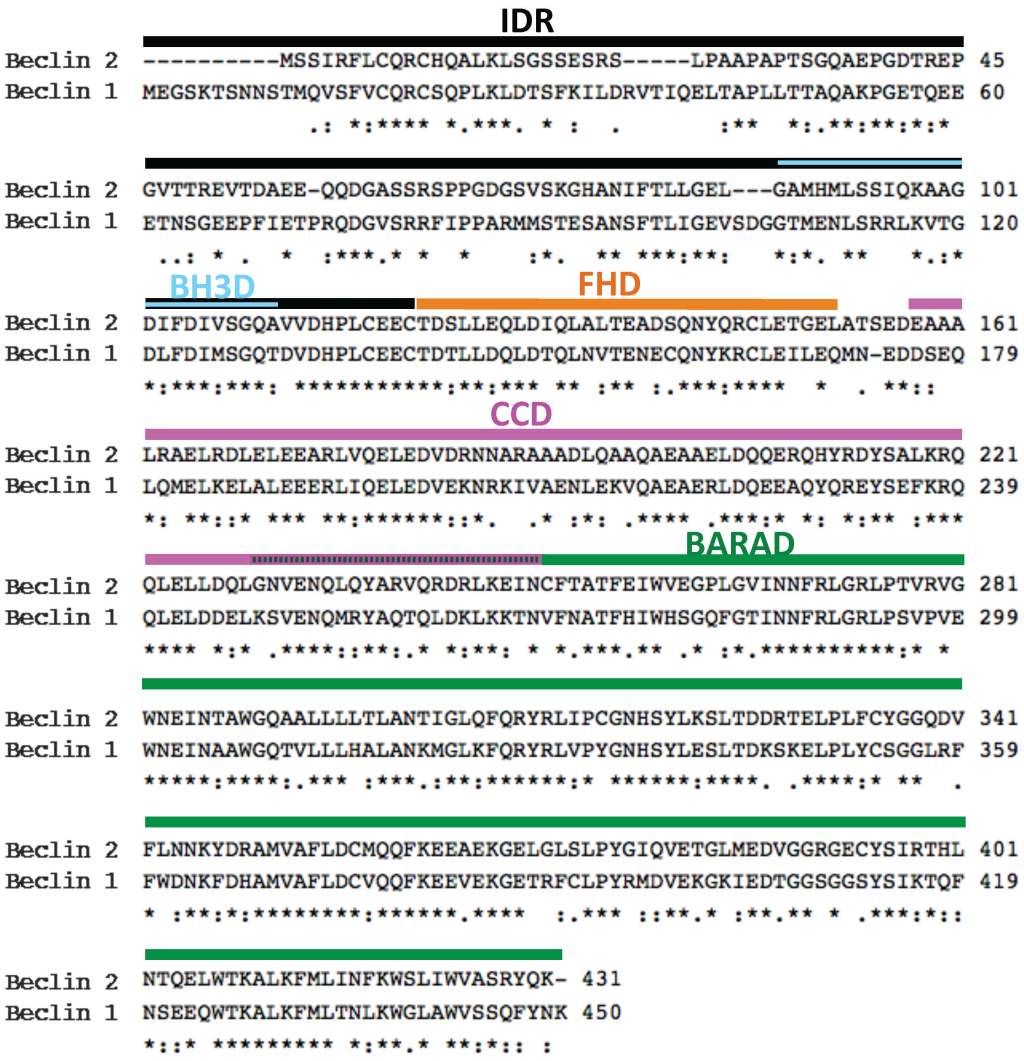

Figure S1: Sequence alignment of human BECN1/Beclin 1 and BECN2/Beclin 2. Asterisks represent identical residues while double and single dots represent decreasing sequence conservation. Domain boundaries are displayed above the alignment with the black, cyan, orange, magenta and green lines representing the IDR, BH3D, FHD, CCD and BARAD respectively.

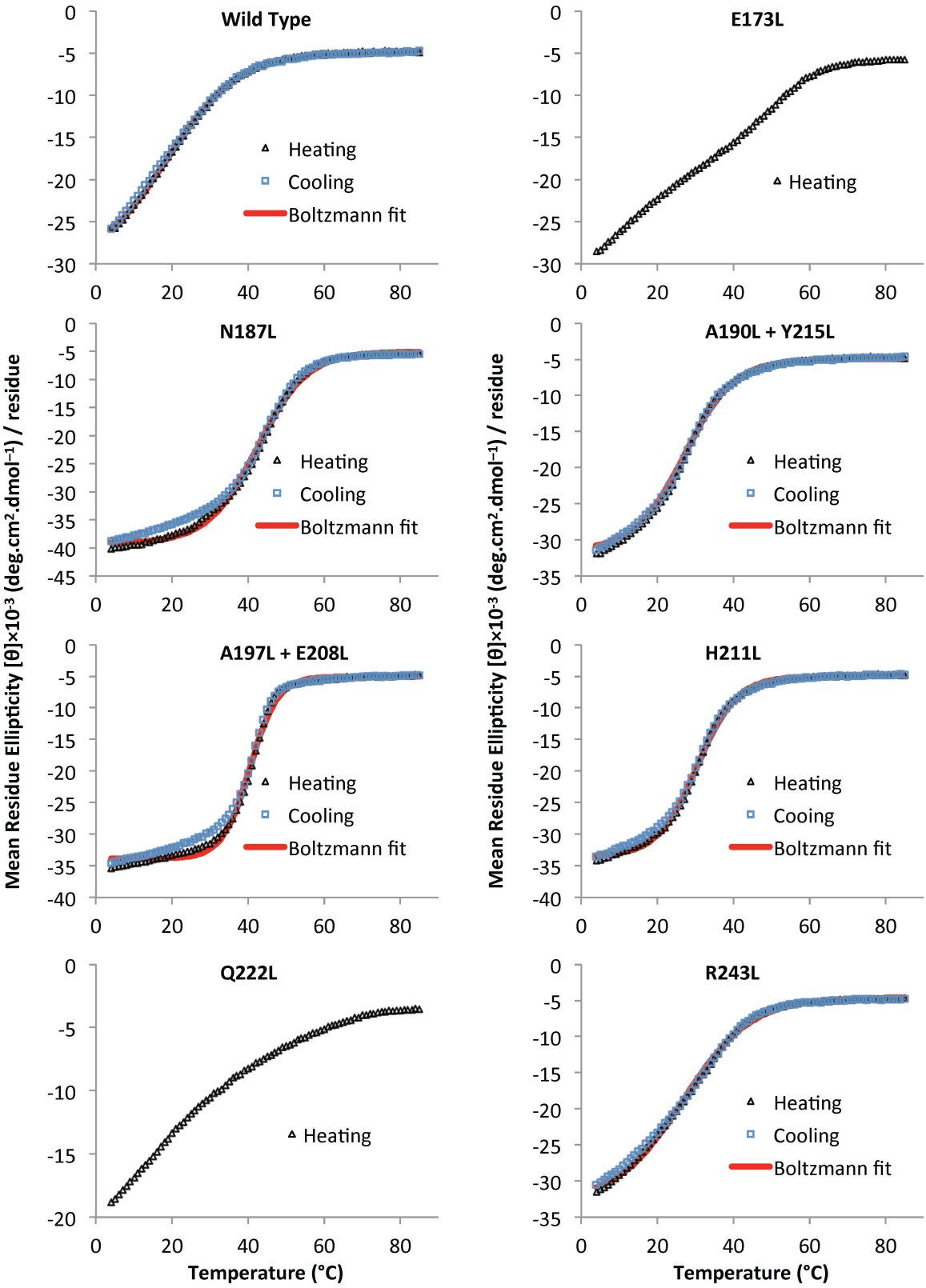

Figure S2: Thermal denaturation curves of WT and mutant BECN2 CCD.

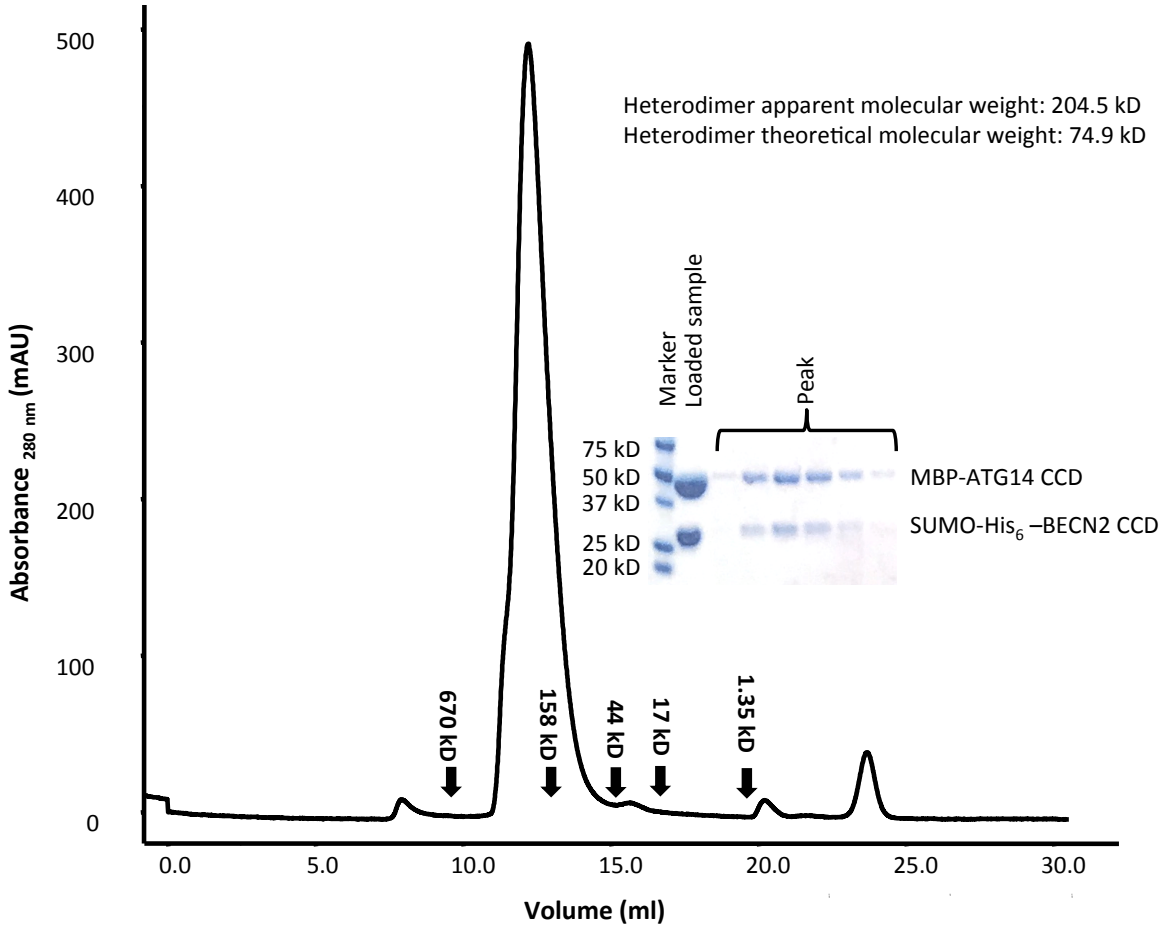

Figure S3: Gel filtration chromatogram and corresponding SDS-PAGE of the SUMO-His$_6$ –BECN2 CCD:MBP-ATG14 CCD complex.

EXPERIMENTAL PROCEDURES

Delineating BECN2 domain architecture

BECN2 domain architecture was delineated using a combination of bioinformatics tools including the alignment of sequences of human BECN1 and BECN2 using ClustalW2[3]; secondary structure prediction using Jpred[4]; and sequence analysis using the programs IUPred[5], PrDOS[6] and the VSL2B algorithm in the PONDR program suite[7; 8] to identify IDRs.

Protein expression and purification

The BECN2 CCD (residues 158-250) was cloned into the *p*MBP parallel 1 expression vector[9] to be expressed as a MBP fusion protein in *E. coli* BL21 (DE3) *p*LysS cells. The soluble protein was first purified by Amylose Affinity Chromatography (AAC), and the MBP-tag was removed by on-column treatment with tobacco etch virus protease. The untagged BECN2 CCD was then purified to homogeneity by Ion Exchange Chromatography using a HR 10/10 Mono Q column (GE Healthcare Life Sciences) followed by SEC using tandem 10/300 GL Superdex 200 and Superdex 75 columns (GE Healthcare Life Sciences). All BECN2 CCD mutants were generated by site-directed mutagenesis and expressed and purified in a manner similar to the WT protein.

The human ATG14 CCD (residues 88-178) was delineated based on the sequence alignment to the rat ATG14 CCD[10], and cloned into the expression vector *p*MBP parallel 1 expression vector[9] with an additional His_6-tag at its C-terminus and expressed in *E. coli* ArcticExpress cells (Agilent Technologies). Soluble MBP-ATG14 CCD-His_6 was purified to homogeneity by AAC followed by Immobilized Metal Affinity Chromatography using two tandem 5 mL His-Trap HP columns (GE Healthcare Life

Sciences) and SEC using a preparative 16/600 Superdex 200 column (GE Healthcare Life Sciences).

Different constructs were used to obtain the BECN2:ATG14 CCD complex for SAXS analysis. A SUMO-His_6-BECN2 CCD construct was created by cloning the His_6-BECN2 CCD coding sequence into a modified *p*ET-28 vector with a SUMO coding sequence preceding the multiple cloning site. The MBP-ATG14 CCD-His_6 construct described above was modified by site directed mutagenesis to replace the long linker between the MBP-tag and ATG14 CCD with a short linker of three alanine residues, and to remove the C-terminal His_6-tag. SUMO-His_6-BECN2 CCD in complex with MBP-ATG14 CCD was expressed in *E. coli* ArcticExpress cells (Agilent Technologies) and purified to homogeneity by Immobilized Metal Affinity Chromatography using 5 mL His-Trap HP columns (GE Healthcare Life Sciences) followed by AAC and SEC using 10/300 Superdex 200 column (GE Healthcare Life Sciences).

Crystallization and structure determination

Both WT and mutant BECN2 CCD proteins were crystallized at 20 °C by hanging-drop vapor diffusion. The WT BECN2 CCD was crystallized from a 1:1 mixture of 5.5 mg/ml protein and reservoir solution comprising 0.1 M Bis-Tris pH 6.5, 0.1 M NaCl and 1.5 M $(NH_4)_2SO_4$. The N187L mutant BECN2 CCD was crystallized from a 1:1 mixture of 12.2 mg/ml protein and reservoir solution comprising of 0.1 M $MgCl_2$ and 19% PEG 3350. All crystals were harvested and cryo-protected in their reservoir solutions plus 25% glycerol and then immediately cryo-cooled in liquid N_2. All diffraction data were collected at 100 K at the 24-ID NE-CAT beam line at the Advanced Photon Source (APS), Argonne National Laboratory (ANL), Argonne, IL. Data were recorded in a 180° sweep from a

single WT BECN2 CCD crystal, at 1 second exposure per 1° crystal rotation per image at a crystal-to-detector distance of 450 mm. Data were also recorded in a 180° sweep from a single N187L BECN2 crystal, at 1 second exposure per 1° crystal rotation per image at a crystal-to-detector distance of 310 mm. The WT BECN2 CCD diffraction data were indexed and integrated using MOSFLM[11]. Various combinations of search models derived from the BECN1 CCD structure (PDB code 3Q8T) were used as the search model for molecular replacement. Ultimately, the WT BECN2 CCD structure was solved by molecular replacement using half of the rat BECN1 CCD homodimer structure, comprising residues 217-265 of one chain and residues 174-219 of the partner chain, as the search model using Phaser-MR in the CCP4 Suite[12]. The initial model contained residues 160-200 in chain A; residues 204-247 in chain B; residues 160-200 in chain C; and residues 203-247 in chain D. Buccaneer in the CCP4 Suite[12] was then used to autobuild the rest of the BECN2 CCD structure. The asymmetric unit contained two BECN2 CCD homodimers, AB and CD (Table 1). For the mutant N187L BECN2 CCD, diffraction data were processed using RAPD automated processing suite (https://rapd.nec.aps.anl.gov/rapd), which incorporates XDS for integration and scaling[13]. The structure of N187L BECN2 CCD was solved by molecular replacement using the WT BECN2 CCD AB homodimer as the search model using Phaser-MR in PHENIX[14]. All refinement was performed using PHENIX. Crystallographic data collection and refinement statistics are summarized in Table 1. All molecular figures were prepared using the PyMOL Molecular Graphics System[15]. Buried surface area was analyzed using PISA[16]. The final refined structures of the WT and the N187L mutant BECN2 CCDs are deposited in the PDB with IDs 5K7B and 5K9L respectively.

ITC

ITC experiments were performed using a Low Volume Nano ITC (TA Instruments). All protein samples were dialyzed against the ITC buffer consisting of 50 mM HEPES, pH 7.5, 150 mM sodium chloride and 2 mM β-mercaptoethanol. All ITC experiments were performed at 15°C with 20 injections of 2.5 μL each, with at least three repeats per measurement. Data were analyzed using the NanoAnalyze Software (TA Instruments), with an independent model for the BECN2 CCD and ATG14 binding experiments and a dimer dissociation model for the BECN2 CCD self-dissociation experiments. For the BECN2 CCD and ATG14 CCD binding experiments, samples were loaded into separate dialysis cassettes, then co-dialyzed into the ITC buffer. The ATG14 CCD was loaded into the syringe and titrated into the cell containing the BECN2 CCD. Self-dissociation experiments were performed by titrating protein into its dialysis buffer. Blank profiles obtained by titrating ATG14 into dialysis buffer or titrating buffer into buffer were subtracted from the experimental profiles of BECN2 CCD and ATG14 CCD binding experiments or BECN2 CCD self-dissociation experiments respectively.

CD

CD data were recorded from the WT and mutant BECN2 CCD at a concentration of 50 μM in a quartz cell with a 0.1 cm path length using a Jasco J-815 CD spectrometer. Each sample was dialyzed into CD buffer comprising 10 mM Potassium phosphate, pH 7.5 and 100 mM ammonia sulfate. Full-length scanning spectra were collected between 200 and 250 nm at 4 °C. Secondary structure content of each sample was estimated using K2D3[2] and SELCON3 within the CDPro program package[1]. Thermal denaturation curves were recorded by measuring CD signal at 222 nm at 1 °C intervals with a ramp rate of 1 °C

/min, from 4 °C to 85 °C for heating (or 85°C to 4 °C for cooling measurements). Data were analyzed using OriginPro 8 (OriginLab). The mean residue molar ellipticity was plotted against temperature and the T_m obtained by fitting data to the Boltzman algorithm included in OriginPro 8. The values reported in Table 3 are the average of T_m calculated separately from heating and cooling curves.

SEC-SAXS

SEC-SAXS data were recorded at beam line 18-ID Bio-CAT at APS, ANL, Argonne, IL. Purified proteins in 20 mM Tris, pH 8.0, 150 mM NaCl and 2 mM β-mercaptoethanol were loaded onto an inline Superdex 200 10/300 SEC column and eluted at 0.8 ml/min. SAXS data were recorded by exposing the column eluate to the X-ray beam for one second with a periodicity of three seconds. The data were recorded on a Pilatus 1M detector at a sample-to-detector distance of 3.5 m, covering a momentum transfer range of $0.0036\ Å^{-1} < q < 0.4\ Å^{-1}$. Scattering data were normalized to the incident X-ray beam intensity, and buffer subtraction was performed prior to processing using the ATSAS program suite[17]. Within the ATSAS program suite, PRIMUS[18] was used to scale and average data for further analysis. The linear Guinier region was estimated using PRIMUS, and the R_g was calculated from Guinier extrapolation. The P(r) plot and Kratky plot were calculated using GNOM[19]. The P(r) plot was used to estimate R_g and D_{max}, and for the calculation of ten independent *ab initio* bead models using DAMMIF[20] which were then sequentially modeled using DAMSEL, DAMSUP, DAMAVER[21] and DAMMFILT. The AMBIMETER score is 1.7, i.e. the 3D reconstruction might be ambiguous. The atomic structures of MBP (extracted from PDB code 4GGQ), SUMO (extracted from PDB code 1L2N) and the BECN2:ATG14 CCD model were used in SASREF[22] to build a model

that was fit into the corresponding SAXS data set. FoXS[23; 24] was used to compare theoretical scattering curves calculated for SUMO-His_6-BECN2:MBP-ATG14 CCD heterodimer models against the experimental SAXS scattering curve, while SUPCOMB[25] was used to superimpose the SUMO-His_6-BECN2:MBP-ATG14 CCD heterodimer models to the *ab initio* bead models.

Construction of an Atomic Model of the BECN2:ATG14 CCD heterodimer

Based on our SAXS data, the BECN2:ATG14 CCD heterodimer model was built as a parallel CCD. CCBuilder[26] was used to build seven heterodimer models by changing the register along the ATG14 sequence, to place successive residues at the *a* and *d* positions. The most optimal of the different packing patterns so produced was selected as the correct register. $(PS)^2$,[27] which builds a model for protein complexes based on considerations of the packing density in the complex and sequence alignments with known structures was then used to further calculate a heterodimer model based on the amino acid sequences of BECN2 CCD and ATG14 CCD and the packing pattern obtained from CCBuilder.

Supplemental References:

1. Sreerama N, Venyaminov SY, Woody RW. 2001. Analysis of protein circular dichroism spectra based on the tertiary structure classification. Analytical biochemistry. 299(2):271-274.
2. Louis-Jeune C, Andrade-Navarro MA, Perez-Iratxeta C. 2012. Prediction of protein secondary structure from circular dichroism using theoretically derived spectra. Proteins: Structure, Function, and Bioinformatics. 80(2):374-381.
3. Larkin MA, Blackshields G, Brown NP, Chenna R, McGettigan PA, McWilliam H, Valentin F, Wallace IM, Wilm A, Lopez R et al. 2007. Clustal W and Clustal X version 2.0. Bioinformatics. 23(21):2947-2948.
4. Cole C, Barber JD, Barton GJ. 2008. The Jpred 3 secondary structure prediction server. Nucleic Acids Research. 36(suppl 2):W197-W201.
5. Dosztányi Z, Csizmok V, Tompa P, Simon I. 2005. IUpred: Web server for the prediction of intrinsically unstructured regions of proteins based on estimated energy content. Bioinformatics. 21(16):3433-3434.
6. Ishida T, Kinoshita K. 2007. Prdos: Prediction of disordered protein regions from amino acid sequence. Nucleic Acids Research. 35:W460-W464.
7. Obradovic Z, Peng K, Vucetic S, Radivojac P, Dunker AK. 2005. Exploiting heterogeneous sequence properties improves prediction of protein disorder. Proteins. 61(S7):176-182.
8. Peng K, Radivojac P, Vucetic S, A.K. D, Obradovic Z. 2006. Length-dependent prediction of protein intrinsic disorder. BMC Bioinformatics. 7:208.
9. Sheffield P, Garrard S, Derewenda Z. 1999. Overcoming expression and purification problems of rhogdi using a family of "Parallel" Expression vectors. Protein Expression and Purification. 15(1):34-39.
10. Li X, He L, Che KH, Funderburk SF, Pan L, Pan N, Zhang M, Yue Z, Zhao Y. 2012. Imperfect interface of Beclin1 coiled-coil domain regulates homodimer and heterodimer formation with ATG14l and UVRAG. Nature communicaitons. 3:662.
11. Leslie AGW, Powell HR. 2007. Processing diffraction data with MOSFLM. In: Read RJ, Sussman JL, editors. Nato Sci ser II math. Dordrecht: Springer Link. p. 41-51.
12. Winn MD, Ballard CC, Cowtan KD, Dodson EJ, Emsley P, Evans PR, Keegan RM, Krissinel EB, Leslie AGW, McCoy A et al. 2011. Overview of the CCP4 suite and current developments. Acta Crystallographica Section D, Biological Crystallography. 67(4):235-242.
13. Kabsch W. 2010. Integration, scaling, space-group assignment and post-refinement. Acta Crystallographica Section D. 66:133-144.
14. Adams PD, Afonine PV, Bunkoczi G, Chen VB, Davis IW, Echols N, Headd JJ, Hung LW, Kapral GJ, Grosse-Kunstleve RW et al. 2010. PHENIX: A comprehensive PYTHON-based system for macromolecular structure solution. Acta Crystallographica Section D, Biological Crystallography. 66(Pt 2):213-221.
15. Schrodinger, LLC. Forthcoming 2015 November. The pymol molecular graphics system, version 1.8.
16. Krissinel E, Henrick K. 2007. Inference of macromolecular assemblies from crystalline state. Journal of Molecular Biology. 372:774-797.
17. Petoukhov MV, Franke D, Shkumatov AV, Tria G, Kikhney AG, Gajda M, Gorba C, Mertens HDT, Konarev PV, Svergun DI. 2012. New developments in the ATSAS

program package for small-angle scattering data analysis. Journal of Applied Crystallography. 45:342-350.
18. Konarev PV, Volkov VV, Sokolova AV, Koch MHJ, Svergun DI. 2003. PRIMUS: A Windows PC-based system for small-angle scattering data analysis. Journal of Applied Crystallography. 36:1277-1282.
19. Svergun DI. 1992. Determination of the regularization parameter in indirect-transform methods using perceptual criteria. Journal of Applied Crystallography. 25(4):495-503.
20. Franke D, Svergun DI. 2009. DAMMIF, a program for rapid *ab-initio* shape determination in small-angle scattering. Journal of Applied Crystallography. 42:342-346.
21. Volkov VV, Svergun DI. 2003. Uniqueness of *ab initio* shape determination in small-angle scattering. Journal of Applied Crystallography. 36:860-864.
22. Petoukhov MV, Svergun DI. 2005. Global rigid body modeling of macromolecular complexes against small-angle scattering data. Biophysical Journal. 89(2):1237-1250.
23. Schneidman-Duhovny D, Hammel M, Sali A. 2010. Foxs: A web server for rapid computation and fitting of SAXS profiles. Nucleic Acids Research. 38:W540-W544.
24. Schneidman-Duhovny D, Hammel M, Tainer JA, Sali A. 2013. Accurate SAXS profile computation and its assessment by contrast variation experiments. Biophysical Journal. 105(4):962-974.
25. Kozin MB, Svergun DI. 2001. Automated matching of high- and low-resolution structural models. Journal of Applied Crystallography. 34:33-41.
26. Wood CW, Bruning M, Ibarra AA, Bartlett GJ, Thomson AR, Sessions RB, Brady RL, Woolfson DN. 2014. Ccbuilder: An interactive web-based tool for building, designing and assessing coiled-coil protein assemblies. Bioinformatics. 30(21):3029-3035.
27. Huang TT, Hwang JK, Chen CH, Chu CS, Lee CW, Chen CC. 2015. (ps)2: Protein structure prediction server version 3.0. Nucleic Acids Research. 43(W1):W338-342.